JACS
JOURNAL OF THE AMERICAN CHEMICAL SOCIETY
Article
pubs.acs.org/JACS

Ga^{3+}/Ln^{3+} Metallacrowns: A Promising Family of Highly Luminescent Lanthanide Complexes That Covers Visible and Near-Infrared Domains

Chun Y. Chow,[†,#] Svetlana V. Eliseeva,[*,‡,#] Evan R. Trivedi,[†,⊥] Tu N. Nguyen,[†] Jeff W. Kampf,[†] Stéphane Petoud,[*,‡,∥] and Vincent L. Pecoraro[*,†]

[†]Department of Chemistry, Willard H. Dow Laboratories, University of Michigan, Ann Arbor, Michigan 48109, United States
[‡]Centre de Biophysique Moléculaire, CNRS UPR 4301, F-45071 Orléans Cedex 2, France

Supporting Information

ABSTRACT: Luminescent lanthanide(III)-based molecular scaffolds hold great promises for materials science and for biological applications. Their fascinating photophysical properties enable spectral discrimination of emission bands that range from the visible to the near-infrared (NIR) regions. In addition, their strong resistance to photobleaching makes them suitable for long duration or repeated biological experiments using a broad range of sources of excitation including intense and focalized systems such as lasers (e.g., confocal microscopy). A main challenge in the creation of luminescent lanthanide(III) complexes lies in the design of a ligand framework that combines two main features: (i) it must include a chromophoric moiety that possesses a large molar absorptivity and is able to sensitize several different lanthanide(III) ions emitting in the visible and/or in the near-infrared, and (ii) it must protect the Ln^{3+} cation by minimizing nonradiative deactivation pathways due to the presence of −OH, −NH and −CH vibrations. Herein, a new family of luminescent Ga^{3+}/Ln^{3+} metallacrown (MC) complexes is reported. The MCs with the general composition $[LnGa_4(shi)_4(C_6H_5CO_2)_4(C_5H_5N)\ (CH_3OH)]$ (**Ln-1**, Ln = Sm^{3+}−Yb^{3+}) were synthesized in a one pot reaction using salicylhydroxamic acid (H_3shi) with Ga^{3+} and Ln^{3+} nitrates as reagents. The molecular structure of $[DyGa_4(shi)_4(C_6H_5CO_2)_4(C_5H_5N)\ (CH_3OH)]$ was obtained by X-ray analysis of single crystals and shows that the complex is formed as a $[12\text{-}MC_{Ga(III)shi}\text{-}4]$ core with four benzoate molecules bridging the central Dy^{3+} ion to the Ga^{3+} ring metals. The powder X-ray diffraction analysis demonstrates that all other isolated complexes are isostructural. The extended analysis of the luminescence properties of these complexes, excited by the electronic states of the chromophoric ligands, showed the presence of characteristic, sharp f−f transitions that can be generated not only in the NIR (Sm, Dy, Ho, Er, Yb) but also in the visible (Sm, Eu, Tb, Dy, Tm). All **Ln-1** complexes possess very high quantum yield values with respect to other literature compounds, indicating a good sensitization efficiency of the $[12\text{-}MC_{Ga(III)shi}\text{-}4]$ scaffold. Especially, as of today, the **Yb-1** complex exhibits the highest NIR quantum yield reported for a lanthanide(III) complex containing C−H bonds with a value of 5.88(2)% in the solid state. This work is a significant step forward toward versatile, easily prepared luminescent lanthanide(III) complexes suitable for a variety of applications including highly in demand biological imaging, especially in the NIR domain.

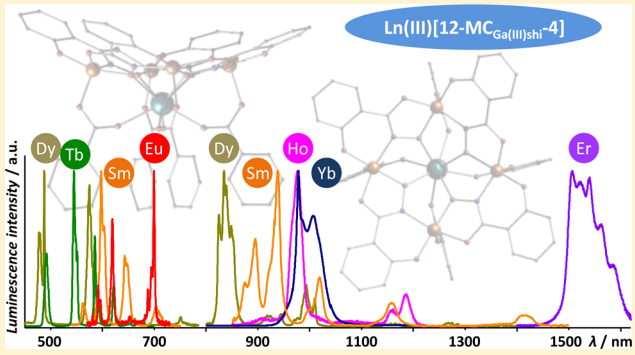

INTRODUCTION

Lanthanide(III) metal ions possess attractive luminescence properties that open new possibilities for a broad range of applications due to their unique electronic configurations. The combination of sharp emission bandwidths, long luminescence lifetimes and stronger resistance to photobleaching makes Ln^{3+} luminescence appealing for a broad range of practical applications such as bioanalysis and biological imaging,[1−5] solar energy conversion,[6−8] diode displays,[9] and telecommunications.[10,11] Lanthanide(III) luminescence bands originate from electronic transitions located within their valence 4f orbitals. Since these 4f orbitals are shielded by the 5s and 5p orbitals,[12] they do not participate significantly in the formation of coordination bonds. As a result, the luminescence of the different Ln^{3+} cations appear as atom-like sharp emission bands, the wavelengths of which are mostly unaffected by the Ln^{3+} coordination environment. This property is advantageous for optical biological imaging due to the efficiency of the spectral discrimination of the lanthanide(III) signal in a complex mixture of fluorescent biological molecules (autofluorescence), leading to a better signal-to-noise ratio and corresponding detection sensitivity. Consequently, a large number of sharp emission bands are available across the visible and near-infrared

Received: January 27, 2016
Published: March 25, 2016

DOI: 10.1021/jacs.6b00984
J. Am. Chem. Soc. 2016, 138, 5100−5109

(NIR) spectral regions, the wavelengths of which depend on the nature of the Ln^{3+}.[13] Since most of these f−f transitions are forbidden by the Laporte rule,[12] the direct excitation of luminescent lanthanide(III) cations is inefficient due to their low molar absorption coefficients. This limitation can be overcome with the help of a highly absorbing "antenna" located in a sufficiently close proximity to the Ln^{3+}.[14] The sensitization through the "antenna effect" implies the excitation of the organic chromophoric moieties by electromagnetic radiation, followed by the transfer of the corresponding energy to the accepting levels of the Ln^{3+} ions. The subsequent Ln^{3+} emission occurs with long luminescence lifetimes upon relaxation of the system back to the ground state. This "antenna" sensitization strategy has led to the development of a wide variety of Ln^{3+}-based luminescent complexes and nanomaterials formed with organic ligands. The specific wavelengths of emission bands in the visible and NIR can be obtained by the choice of Ln^{3+} ions across the lanthanide series.[13] The energy difference (ΔE) between the ligand excited triplet state (T_1) and the accepting electronic level corresponding to the f-orbital located on the lanthanide(III) is one of the identified parameters that impacts the global sensitization efficiency. Some families of sensitizing moieties have been identified as more efficient for the Ln^{3+} ions emitting in the visible (Tb^{3+}, Sm^{3+}, Dy^{3+}, Eu^{3+})[15,16] while others are more suitable for those emitting in the NIR (Nd^{3+}, Er^{3+}, Ho^{3+}, Yb^{3+}, Tm^{3+}).[17,18] To date, only a very limited selection of ligand systems has been demonstrated to be able to sensitize Ln^{3+} across the entire spectrum.[19−22]

Metallacrowns (MCs) are metal-rich macrocycles that form repeating [Metal−N−O] subunits.[23,24] Analogous to organic crown ethers, these MC complexes possess oxygen atoms that are oriented toward the interior of the macrocyclic ring, which is preorganized for guest encapsulation in a manner similar to classical organic crown ethers. Accordingly, MCs bind a central metal cation through these oxygen coordination sites. Moreover, ligands that bind the central and ring metals, such as carboxylic acid groups, provide additional stability for the complex. The MC approach offers an appealing route towards the a priori design of multimetallic complexes. This platform-oriented strategy has been used to spatially organize transition metals and lanthanide ions in a rigid framework formed by core−shell structures to explore applications in anion recognition,[25−28] molecular magnetism,[29−35] and more recently, in lanthanide-based luminescence.[36,37]

We have recently reported the first examples of Ln^{3+} NIR luminescence from a MC motif based on closed-shell Zn^{2+} ions and bivalent aromatic hydroximate ligands (L^{2-}).[36,37] In these structures, a single Ln^{3+} cation is sandwiched between two [12-MC-4] MCs and is further encapsulated by an additional [24-MC-8] MC, leading to an overall stoichiometry of $LnZn_{16}L_{16}$. $LnZn_{16}L_{16}$ MCs have demonstrated remarkable NIR luminescence properties, showing the highest luminescence quantum yield values reported at this time for NIR-emitting Er^{3+} and Nd^{3+} analogues in the solid state and in deuterated methanol.[36] However, the type of organic antenna present on this family of molecules and their arrangement leading to the formation of inter- and/or intraligand charge transfer states led to the inability to sensitize Ln^{3+} other than Yb^{3+}, Nd^{3+}, and Er^{3+}. A major objective of our present work is the sensitization of a larger number of Ln^{3+} ions using a single MC scaffold in order to access multiple emission colors in the visible and/or in the NIR, a broad range of lifetimes and efficient quantum yields with a single excitation wavelength.

One of the simplest of metallacrown structures is the 12-MC-4 structure. We have previously shown that mixed valence $(Mn(II)\ (OAc)_2[12\text{-}MC_{Mn(III)N}\text{-}4])$[32,38] and mixed metal $(M(I)Ln(III)\ (OAc)_4[12\text{-}MC_{Mn(III)N}\text{-}4])$[39] complexes could be prepared in high yield with predictable structures using the organic ligand salicylhydroximate (shi^{3-}). While these lanthanide(III) compounds were successful single molecule magnets, they were ineffective for luminescence studies, presumably due to the manganese(III) ring metals. For this reason, we explored the preparation of the same 12-MC-4 platform using the colorless and diamagnetic Ga^{3+} ion, whose positive charge compensates the charge of the trivalent shi^{3-} ligand, and should yield an isostructural and similarly charged compound. Herein, we present the syntheses, structures and photophysical properties of a series of novel Ga^{3+}/Ln^{3+} MCs with the general composition $[LnGa_4(shi)_4(C_6H_5CO_2)_4(C_5H_5N)\ (CH_3OH)]$ (**Ln-1**, Ln = Sm^{3+}−Yb^{3+}). Detailed studies of the photophysical parameters of the Ln^{3+}- as well as ligand-centered transitions of these MC complexes will be discussed.

EXPERIMENTAL SECTION

All reagents and chemicals were purchased from commercial sources and used without further purification. All reactions were carried under aerobic conditions. Elemental analysis was performed by Atlantic Microlabs Inc.

Preparation of Ln-1 Complexes. Three different procedures were used for the synthesis of the **Ln-1** complexes depending on the nature of the Ln^{3+} ion.

Sm-1 and Eu-1. H_3shi (153.1 mg, 1.0 mmol), $Ln(NO_3)_3{\cdot}xH_2O$ (0.5 mmol) (Ln^{3+}= Sm^{3+}, Eu^{3+}), and $Ga(NO_3)_3{\cdot}xH_2O$ (255.7 mg, 1.0 mmol) were dissolved in 40 mL of methanol. Sodium benzoate (432.3 mg, 3.0 mmol) was added to the solution and the mixture was stirred overnight. The solution was filtered and 2 mL pyridine were added. The resulting solution was stirred for 15 min and then filtered. The slow evaporation of the solution yielded the collection of a crystalline compound after 2 weeks.

Gd-1, Tb-1, Dy-1, Ho-1, Er-1. H_3shi (153.1 mg, 1.0 mmol), $Ln(NO_3)_3{\cdot}xH_2O$ (0.25 mmol) (Ln^{3+}= Gd^{3+}, Tb^{3+}, Dy^{3+}, Ho^{3+}, Er^{3+}), and $Ga(NO_3)_3{\cdot}xH_2O$ (255.7 mg, 1.0 mmol) were dissolved in 40 mL of methanol. Sodium benzoate (432.3 mg, 3.0 mmol) was added to the solution and the mixture was stirred overnight. The solution was filtered and 2 mL of pyridine were added to the filtrate. The resulting solution was stirred for 15 min and then filtered. Slow evaporation of the solution yielded the formation of a crystalline compound after 2 weeks.

Tm-1 and Yb-1. H_3shi (153.1 mg, 1.0 mmol), $Ln(NO_3)_3{\cdot}xH_2O$ (0.25 mmol) (Ln^{3+} = Tm^{3+}, Yb^{3+}), and $Ga(NO_3)_3{\cdot}xH_2O$ (255.7 mg, 1.0 mmol) were dissolved in 40 mL of methanol. Sodium benzoate (576.4 mg, 4.0 mmol) was added to the solution and the mixture was stirred overnight. The solution was filtered, followed by the addition of 2 mL pyridine. The resulting solution was stirred for 15 min and then filtered. The slow evaporation of the solution yielded crystalline compound after 2 weeks.

$[SmGa_4(shi)_4(C_6H_5CO_2)_4(C_5H_5N)\ (CH_3OH)]{\cdot}C_5H_6N{\cdot}C_5H_5N{\cdot}CH_3OH$ (**Sm-1**). Yield: 104.9 mg (23.1%). ESI-MS, calc. for $[M]^-$, $C_{56}H_{36}N_4O_{20}SmGa_4$, 1519.8; found, 1519.8. Anal. Calc. for $SmGa_4C_{73}H_{60}N_7O_{22}$: C, 48.27; H, 3.33; N, 5.40. Found: C, 48.29; H, 3.16; N, 5.51.

$[EuGa_4(shi)_4(C_6H_5CO_2)_4(C_5H_5N)\ (CH_3OH)]{\cdot}C_5H_6N{\cdot}C_5H_5N{\cdot}CH_3OH$ (**Eu-1**). Yield: 213.0 mg (46.8%). ESI-MS, calc. for $[M]^-$, $C_{56}H_{36}N_4O_{20}EuGa_4$, 1519.8; found, 1519.8. Anal. Calc. for $EuGa_4C_{73}H_{60}N_7O_{22}$: C, 48.22; H, 3.33; N, 5.39. Found: C, 48.35; H, 3.13; N, 5.58.

$[GdGa_4(shi)_4(C_6H_5CO_2)_4(C_5H_5N)\ (CH_3OH)]{\cdot}C_5H_6N{\cdot}C_5H_5N{\cdot}CH_3OH$ (**Gd-1**). Yield: 91.8 mg (20.1%). ESI-MS, calc. for $[M]^-$, $C_{56}H_{36}N_4O_{20}GdGa_4$, 1519.8; found, 1519.8. Anal. Calc. for

DOI: 10.1021/jacs.6b00984
J. Am. Chem. Soc. 2016, 138, 5100−5109

$GdGa_4C_{73}H_{60}N_7O_{22}$: C, 48.09; H, 3.32; N, 5.38. Found: C, 48.18; H, 3.07; N, 5.57.

$[TbGa_4(shi)_4(C_6H_5CO_2)_4(C_5H_5N)\ (CH_3OH)]\cdot C_5H_6N\cdot C_5H_5N\cdot CH_3OH$ (**Tb-1**). Yield: 102.0 mg (22.4%). ESI-MS, calc. for $[M]^-$, $C_{56}H_{36}N_4O_{20}TbGa_4$, 1522.8; found, 1522.8. Anal. Calc. for $TbGa_4C_{73}H_{60}N_7O_{22}$: C, 48.04; H, 3.31; N, 5.37. Found: C, 48.33; H, 3.12; N, 5.54.

$[DyGa_4(shi)_4(C_6H_5CO_2)_4(C_5H_5N)\ (CH_3OH)]\cdot C_5H_6N\cdot C_5H_5N\cdot CH_3OH$ (**Dy-1**). Yield: 106.6 mg (23.3%). ESI-MS, calc. for $[M]^-$, $C_{56}H_{36}N_4O_{20}DyGa_4$, 1525.8; found, 1525.8. Anal. Calc. for $DyGa_4C_{73}H_{60}N_7O_{22}$: C, 47.95; H, 3.31; N, 5.36. Found: C, 48.08; H, 3.10; N, 5.54.

$[HoGa_4(shi)_4(C_6H_5CO_2)_4(C_5H_5N)\ (CH_3OH)]\cdot C_5H_6N\cdot C_5H_5N\cdot CH_3OH$ (**Ho-1**). Yield: 160.4 mg (35.0%). ESI-MS, calc. for $[M]^-$, $C_{56}H_{36}N_4O_{20}HoGa_4$, 1528.8; found, 1529.3. Anal. Calc. for $HoGa_4C_{73}H_{60}N_7O_{22}$: C, 47.88; H, 3.30; N, 5.35. Found: C, 48.01; H, 3.07; N, 5.50.

$[ErGa_4(shi)_4(C_6H_5CO_2)_4(C_5H_5N)\ (CH_3OH)]\cdot C_5H_6N\cdot 0.5C_5H_5N$ (**Er-1**). Yield: 159.5 mg (36.2%). ESI-MS, calc. for $[M]^-$, $C_{56}H_{36}N_4O_{20}ErGa_4$, 1529.8; found, 1530.1. Anal. Calc. for $ErGa_4C_{69.5}H_{53.5}N_{6.5}O_{21}$: C, 47.38; H, 3.06; N, 5.17. Found: C, 47.29; H, 3.05; N, 5.53.

$[TmGa_4(shi)_4(C_6H_5CO_2)_4(C_5H_5N)\ (CH_3OH)]\cdot C_5H_6N\cdot 0.5C_5H_5N$ (**Tm-1**). Yield: 148.4 mg (33.6%). ESI-MS, calc. for $[M]^-$, $C_{56}H_{36}N_4O_{20}TmGa_4$, 1532.8; found, 1532.8. Anal. Calc. for $TmGa_4C_{69.5}H_{53.5}N_{6.5}O_{21}$: C, 47.33; H, 3.06; N, 5.16. Found: C, 47.06; H, 2.95; N, 5.48.

$[YbGa_4(shi)_4(C_6H_5CO_2)_4(C_5H_5N)\ (CH_3OH)]\cdot C_5H_6N\cdot C_5H_5N\cdot CH_3OH$ (**Yb-1**). Yield: 54.1 mg (11.8%). ESI-MS, calc. for $[M]^-$, $C_{56}H_{36}N_4O_{20}YbGa_4$, 1535.8; found, 1535.8. Anal. Calc. for $YbGa_4C_{73}H_{60}N_7O_{22}$: C, 47.67; H, 3.29; N, 5.33. Found: C, 47.69; H, 3.10; N, 5.49.

X-ray Crystallography. Single-crystal X-ray crystallographic data for **Dy-1** were collected at 85(2) K on an AFC10K Saturn 944+ CCD-based X-ray diffractometer equipped with a Micromax007HF Cu-target microfocus rotating anode (λ = 1.54187 Å), operated at 1200 W power (40 kV, 30 mA). The data were processed with CrystalClear 2.0[40] and corrected for the absorption. The structure was solved and refined with the SHELXTL (version 6.12) software package.[41] All non-hydrogen atoms were refined anisotropically. Hydrogen atoms were placed in their idealized positions. Experimental parameters and crystallographic data for **Dy-1** are provided in Table S1.

Powder X-ray Diffraction (PXRD). Powder X-ray diffraction data for air-dried samples of the **Ln-1** complexes were collected at room temperature using a Bruker D8 Advance diffractometer with Cu Kα radiation (1.5406 Å, 40 kV, 40 mA) from 3° to 50° (2θ) using a step size of 0.05° and a scan rate of 0.5 s/step.

Photophysical Measurements. Luminescence data were collected on samples placed in 2.4 mm i.d. quartz capillaries. Emission and excitation spectra were measured on a custom-designed Horiba Scientific Fluorolog 3 spectrofluorimeter equipped with either a visible photomultiplier tube (PMT) (220–850 nm, R928P; Hamamatsu), a NIR solid-state InGaAs detector cooled to 77 K (800–1600 nm, DSS-IGA020L; Horiba Scientific), or a NIR PMT (950–1650 nm, H10330–75; Hamamatsu). Excitation and emission spectra were corrected for instrumental functions. Luminescence lifetimes were determined under excitation at 355 nm provided by a Nd:YAG laser (YG 980; Quantel). Signals were detected in the NIR with the help of a Hamamatsu H10330–75 PMT. The output signals from the detectors were fed into a 500 MHz bandpass digital oscilloscope (TDS 754C; Tektronix), transferred to a PC for data processing with the program Origin 8. Luminescence lifetimes are averages of at least three independent measurements. Quantum yields were determined with the Fluorolog 3 spectrofluorimeter based on an absolute method with the use of an integration sphere (Model G8, GMP SA, Renens, Switzerland). Each sample was measured several times under comparable experimental conditions, varying the position of samples. Estimated experimental error for quantum-yield determination is ~10%.

Absorption Spectroscopy. Solid-state UV–vis spectra were collected using an Agilent-Cary 5000 spectrophotometer equipped with a Praying Mantis diffuse reflectance accessory. Spectra were collected in the reflectance (R) mode, the signal of pure $BaSO_4$ was used as the baseline. Samples (10 wt %) were milled in $BaSO_4$ (90 wt %). The spectra were then converted to represent absorbance using Kubelka–Munk function ($(1-R)^2/2R$). Solution UV–vis spectra for the compounds dissolved in CH_3OH were recorded on a Cary 100Bio UV–vis spectrophotometer in absorbance mode or on a Jasco V670 spectrophotometer.

ESI-Mass Spectrometry. ESI-MS spectra were collected with a Micromass LCT time-of-flight electrospray mass spectrometer in negative ion mode at cone voltages ranging from −40 to −70 V on samples dissolved in DMF. Samples were injected via a syringe pump. Data were processed with the program MassLynx 4.0.

RESULTS

Syntheses. The reaction between H_3shi, nitrates of Ga^{3+} and Ln^{3+}, and sodium benzoate in the CH_3OH/pyridine mixture resulted in the formation of **Ln-1** complexes (Scheme 1) that can be compared to a previously reported manganese

Scheme 1. Synthesis of Ln-1

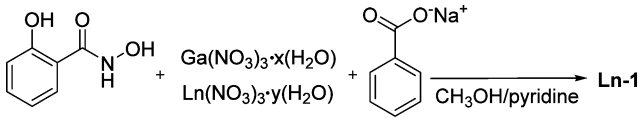

12-MC-4 topology.[39] The synthetic conditions depend strongly on the size of the Ln^{3+} ions, with Sm^{3+} being the largest ion that could be used for the formation of the **Ln-1** MC structure.

Molecular Structure of Ln-1. Crystals of **Dy-1** of suitable size and quality for X-ray diffraction were obtained and analyzed. In parallel, PXRD analysis indicated that nine **Ln-1** MCs are isostructural (Ln^{3+} = Sm^{3+}, Eu^{3+}, Gd^{3+}, Tb^{3+}, Dy^{3+}, Ho^{3+}, Er^{3+}, Tm^{3+}, Yb^{3+}; Figure S1, Supporting Information) allowing a global discussion of the molecular structures of these complexes.

The crystal structure of **Dy-1** is shown in Figure 1. **Dy-1** crystallized in the monoclinic $P2_1/n$ space group. The 12-MC-4 core of **Dy-1** consists of four Ga^{3+} ions bridged by four shi^{3-} ligands in a nearly planar geometry. The central Dy^{3+} ion is bridged to the central ring by four benzoate ligands and adopts an 8-coordinate square antiprism geometry (Figure 1, right), which was confirmed by the SHAPE analysis (Table S2, Supporting Information).[42] This planarity of the 12-MC-4 ring is closely similar to the Mn(II) $(OAc)_2[12\text{-}MC_{Mn(III)N}\text{-}4]$ and slightly more planar than Na(I)Ln(III) $(benzoate)_4[12\text{-}MC_{Mn(III)N}\text{-}4]$ or K(I)Ln(III) $(benzoate)_4[12\text{-}MC_{Mn(III)N}\text{-}4]$. The four Ga^{3+} ions are crystallographically inequivalent; however, the molecule possesses a pseudo-C_4 symmetry. The negative charge of the 12-MC-4 metallacrown is balanced by one pyridinium cation, which was found to form a hydrogen bond with an adjacent pyridine solvent molecule (Figure S2, Supporting Information).

Photophysical Properties. *Ligand-Centered Photophysical Properties.* The absorption and diffuse reflectance spectra of the ligand H_3shi, of the sodium benzoate, and of the corresponding **Ln-1** complexes were studied in both solid state and solution.

In methanol solution, the ligand H_3shi exhibits a broad absorption band attributed to $\pi \rightarrow \pi^*$ transitions located at energies corresponding to the UV region up to 340 nm, with an

DOI: 10.1021/jacs.6b00984
J. Am. Chem. Soc. 2016, 138, 5100–5109

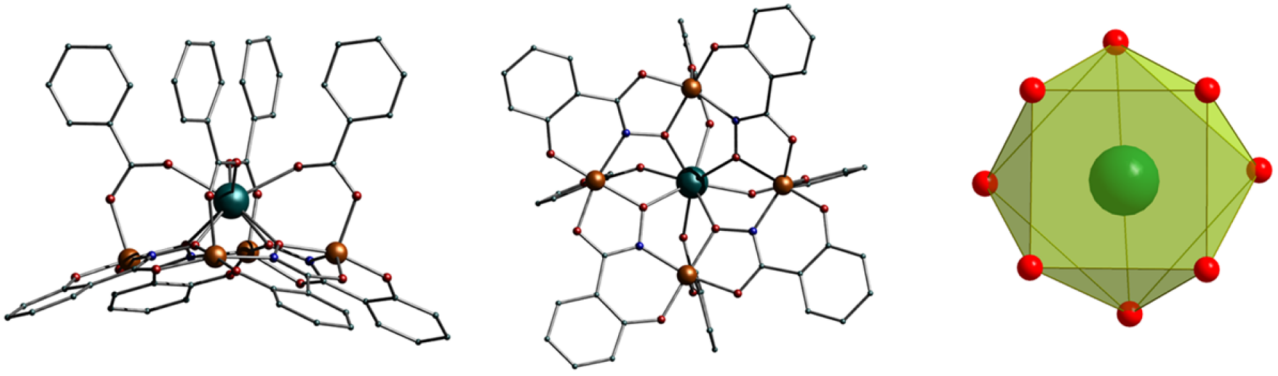

Figure 1. Molecular structure of **Dy-1** obtained from X-ray diffraction: (left) side-view and (middle) top-down view of the 12-MC-4 core. (right) Coordination geometry around the central Dy^{3+} ion. Green sphere, Dy; orange sphere, Ga; red, O; blue, N; greenish gray, C. The hydrogen atoms and solvent molecules coordinated to Ga^{3+} have been omitted for clarity.

additional lower-energy located band centered at ~300 nm (ε = 3.9 × 10^3 M^{-1} cm^{-1}, Figure 2).

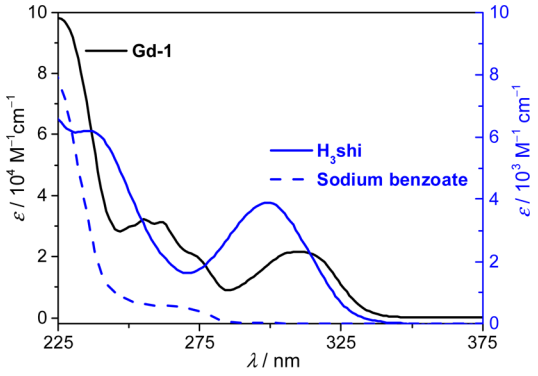

Figure 2. Comparison between the absorption spectra of the complex **Gd-1** (black trace, left scale) and those corresponding to the ligand H_3shi and the sodium benzoate (blue traces, right scale). All spectra were recorded at room temperature in methanol.

The formation of the **Ln-1** MC scaffold induces a red shift of the absorption bands and an increase of the molar absorption coefficients ($\varepsilon_{Gd\text{-}1}$ = 2.16 × 10^4 M^{-1} cm^{-1} at 311 nm). In the solid state, the diffuse reflectance spectra represented as Kubelka–Munk functions of the **Ln-1** complexes exhibit several important and broad ligand-based bands in the range of 200–400 nm, with sharp features of significantly lower contributions at longer wavelengths (above 400 nm). These narrow bands can be unambiguously assigned to the f–f transitions of the corresponding Ln^{3+}: Sm^{3+}, Ho^{3+}, Er^{3+}, and Tm^{3+} (Figure S3, right, Supporting Information). In most cases, the nature of the Ln^{3+} ion does not affect the electronic properties of organic ligands except for the **Eu-1**, for which a significant extension of the ligand-based reflectance band toward longer wavelengths was detected in the solid state as an indication of the presence of ligand-to-metal charge transfer (LMCT) states (Figure S3, Supporting Information). The corresponding LMCT band cannot be observed when recording absorption spectra in solution, due to its low molar absorption coefficient.[43]

Gd^{3+} complexes are convenient probes to assess the organic electronic structure of MCs, including the energies of the triplet states located on their constituting ligands, since the Gd^{3+} ion possesses an accepting electronic level (32 000 cm^{-1}) that is located at sufficiently high energy to prevent any population through energy transfer from the donating electronic levels of the shi^{3-} ligand. Upon excitation of the **Gd-1** MC at 325 nm, the phosphorescence originating from the triplet state located on the ligand was observed by recording emission spectra in time-resolved mode, in the solid state at 77 K and using a 100 μs delay after the excitation flash (Figure 3). The zero-phonon

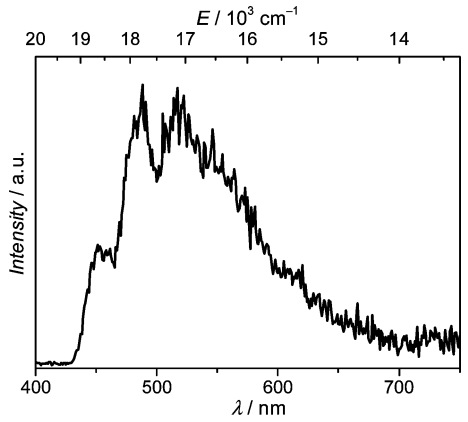

Figure 3. Phosphorescence spectra of **Gd-1** recorded in the solid state under ligand excitation at 325 nm (77 K, 100 μs delay after the excitation flash).

component present on the phosphorescence spectrum best represents the energy of the triplet state (T_1) and was determined to be ~22 170 cm^{-1}, corresponding to an emission band located at 451 nm.

Lanthanide-Centered Photophysical Properties. The excitation and emission spectra of all **Ln-1** complexes were collected both in the solid state and in solution. The excitation spectra of the **Ln-1** compounds collected upon monitoring the main transitions of the corresponding Ln^{3+} are dominated by broad ligand-centered bands located up to 350–400 nm (Figure 4). Due to saturation effects,[44] a slight extension of the ligand-centered excitation bands toward longer wavelengths was observed when compared to the corresponding diffuse reflectance or absorption bands (Figure S4, Supporting Information). For the solid state samples, the sharp characteristic bands with different relative intensities attributed to f–f transitions can also be observed for almost all **Ln-1** complexes except for **Yb-1** (Figure 4). The good match between the absorption/diffuse reflectance and excitation spectra demon-

DOI: 10.1021/jacs.6b00984
J. Am. Chem. Soc. 2016, 138, 5100–5109

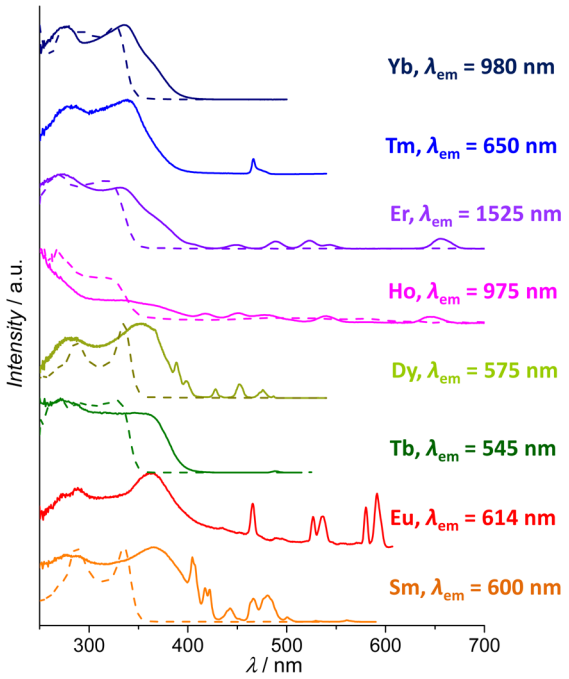

Figure 4. Excitation spectra of the **Ln-1** MCs collected under monitoring the main emission bands of the corresponding Ln^{3+} ions in the solid state (solid traces) and in CD_3OD solution (1 mg/mL, dashed traces) at room temperature.

strates an efficient sensitization of Ln^{3+} ions through the electronic structure of the organic ligands of the MC scaffold.

Upon excitation in the ligand-centered transitions (range of wavelengths 320−350 nm), the characteristic emission bands of the corresponding Ln^{3+} in the visible (Tm^{3+}, Tb^{3+}, Eu^{3+}), NIR (Ho^{3+}, Er^{3+}, Yb^{3+}) or in both ranges (Sm^{3+}, Dy^{3+}) could be observed (Figure 5). Emission spectra were collected for samples in the solid state, in CH_3OH (spectra not shown) and in CD_3OD solution (Figure 5). Luminescence lifetimes and absolute quantum yields (Q_{Ln}^{L}) were also acquired. These results are summarized in Table 1.

For **Sm-1**, the emission spectra recorded in both solid state and in solution display bands in the visible (550−750 nm) and in the NIR (850−1500 nm) ranges that arise from the $^4G_{5/2}$ − ^6H_J (J = 5/2−11/2) and $^4G_{5/2}$ − ^6F_J (J = 1/2−11/2) transitions. Quantum yields up to 2.46/2.33% and 0.45/0.30% for the visible/NIR emission, respectively, were determined in the solid state/CD_3OD. Long luminescence lifetimes, up to 255 μs in CD_3OD solution were recorded for this Sm^{3+} complex. In CH_3OH, the luminescence lifetime and quantum yield values drop by 1 order of magnitude, which can be expected due to the presence of C−H and O−H oscillators that quench the luminescence of the lanthanides. As the sharp emission bands originating from the f−f transitions can be easily discriminated in the excitation spectrum of the solid **Sm-1** (Figure 4, orange solid trace), the determination of the intrinsic quantum yield, Q_{Sm}^{Sm} (5.1(2)%), could be obtained through the direct excitation of the $^4G_{5/2} \leftarrow {}^4I_{9/2,\ 11/2}$ transitions at 480 nm.

Eu-1 exhibits a faint red emission in the solid state due to transitions between $^5D_0$ and ^7F_J (J = 0−4) states in the range of 550−725 nm. The emission spectrum is dominated by the $^5D_0 \rightarrow {}^7F_{2,4}$ transitions. The relatively small quantum yield value and short luminescent lifetimes observed are likely due to the quenching induced by the presence of the LMCT state described previously (vide infra) which is located at sufficiently low energy. In solution, the emission arising from the **Eu-1** complex was too faint to be detected.

The **Tb-1** MC displays a strong green emission resulting from transitions between the $^5D_4$ and ^7F_J (J = 6−0) electronic levels with a quantum yield value of 34.7% in the solid state. The quantum yield decreases by factors of 1.2 and 1.5 when the **Tb-1** MC is placed in CD_3OD or in CH_3OH solutions, respectively. In contrast, the luminescence lifetimes have surprisingly increased by factors of 2 and 1.5 (Table 1).

The emission spectrum of the **Dy-1** MC recorded on solid state samples exhibits several sharp bands across the visible and NIR regions, originating mainly from electronic transitions occurring between the excited $^4F_{9/2}$ and ^6H_J (J = 15/2−5/2) or ^6F_J (J = 9/2−1/2) electronic levels. In the visible range, the spectrum is dominated by two bands which correspond to the $^4F_{9/2} \rightarrow {}^6H_{15/2,\ 13/2}$ transitions and that are responsible for the yellow-green emission of this MC. In solution, an additional residual emission signal arising from the organic ligands was also observed, indicating an incomplete energy transfer from the chromophoric moiety to Dy^{3+} or of the presence of an energy back transfer from Dy^{3+} to the chromophoric ligands. Quantum yield values recorded in the solid state over the

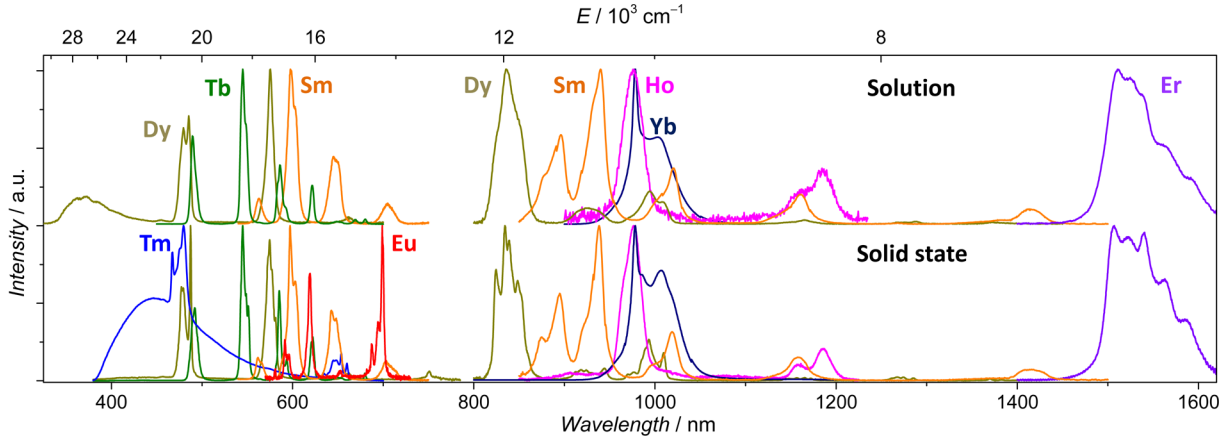

Figure 5. Corrected and normalized emission spectra of the **Ln-1** MCs in the solid state and in CD_3OD solution (1 mg/mL) under ligand excitation at 320−350 nm at room temperature.

DOI: 10.1021/jacs.6b00984
J. Am. Chem. Soc. 2016, 138, 5100−5109

Table 1. Photophysical Data for Ln-1 Complexes under Ligand Excitation at Room Temperature[a]

complex	state/solvent	ΔE (cm^{-1})[b]	τ_{obs} (μs)	q	Q^L_{Ln} (%): vis[c]	Q^L_{Ln} (%): NIR
Sm-1	Solid	4320	148(1)		2.46(8)	$4.50(4)\cdot10^{-1}$
	CD_3OD		255(1)	0.8[d]	2.33(5)	$2.98\ (1)\cdot10^{-1}$
	CH_3OH		26.7(1)		$2.52(2)\cdot10^{-1}$	$2.65(6)\cdot10^{-2}$
Eu-1	Solid	4930	242(7): 79% 43(2): 21%		$1.59(4)\cdot10^{-2}$	–
Tb-1	Solid	1770	1080(10)		34.7(1)	–
	CD_3OD		1960(10)	1.2[e]	28.6(1)	–
	CH_3OH		1510(10)	0.9[f]	23.7(3)	–
Dy-1	Solid	1070	21.2(2)		1.23(2)	0.21(1)
	CD_3OD		25.5(7)	0.7[g]	0.78(1)[1.45(3)]	$6.0(1)\cdot10^{-2}$
	CH_3OH		12.0(1)		0.38(1)[0.70(2)]	$2.4(1)\cdot10^{-2}$
Ho-1	Solid	6670	0.029(1)		–	$2.0(2)\cdot10^{-3}$
	CD_3OD		0.015(1)		–	$1.0(1)\cdot10^{-3}$
Er-1	Solid	15 470	6.75(3)		–	$4.4(1)\cdot10^{-2}$
	CD_3OD		1.74(1)		–	$4.5(3)\cdot10^{-2}$
Tm-1	Solid	820	1.47(1)		0.02(1)[0.12(1)]	–
Yb-1	Solid	11 870	55.7(3)		–	5.88(2)
	CD_3OD		36.6(1)	0.7[h]	–	4.29(1)
	CH_3OH		2.06(4)		–	0.26(1)

[a] 2σ values are given between parentheses; they refer to the reproducibility of the measurements. Experimental relative errors: τ_{obs}, ± 2%; Q^L_{Ln}, ± 10%. [b] $\Delta E(T_1-E^{Ln})$ is the energy gap between the ligand triplet state (T_1 = 22 170 cm^{-1} for **Ln-1**) and Ln^{3+} emissive state: $E^{Sm}(^4G_{5/2})$ = 17 900 cm^{-1}, $E^{Eu}(^5D_0)$ = 17 260 cm^{-1}, $E^{Tb}(^5D_4)$ = 20 400 cm^{-1}, $E^{Dy}(^4F_{9/2})$ = 21 100 cm^{-1}, $E^{Ho}(^5F_5)$ = 15 500 cm^{-1}, $E^{Er}(^4I_{13/2})$ = 6700 cm^{-1}, $E^{Tm}(^1G_4)$ = 21 350 cm^{-1}, $E^{Yb}(^2F_{5/2})$ = 10 300 cm^{-1}.[45,46] [c] Quantum yield of Ln^{3+}-centered transitions. In case ligand emission was observed, total quantum yield is given in square brackets. [d] $q_{Sm} = 2 \times [25.4 \times (k_{CH_3OH} - k_{CD_3OD}) - 0.37]$ in μs.[47] [e] $q_{Tb} = 8.2 \times (k_{CH_3OH} - k_{CD_3OD})$ in ms.[48] [f] $q_{Tb} = 10.0 \times (k_{CH_3OH} - k_{CD_3OD} - 0.06)$ in ms.[49] [g] $q_{Dy} = 2 \times [21.1 \times (k_{CH_3OH} - k_{CD_3OD}) - 0.6]$ in μs.[47] [h] $q_{Yb} = 2 \times (k_{CH_3OH} - k_{CD_3OD} - 0.1)$ in μs.[49]

visible and the NIR ranges are 1.23(1) and 0.21(1) %, respectively.

The infrequently observed NIR emission of Ho^{3+} in **Ho-1** was observed at 965−990 nm and at 1160−1190 nm originating from the $^5F_5 \rightarrow {}^5I_7$ and $^5I_6 \rightarrow {}^5I_8$ transitions, respectively. The quantum yield of **Ho-1** in the solid-state was determined to be $2.0(2)\cdot10^{-3}$ %. This value decreases by half when measured in CD_3OD solution. In CH_3OH, the emission signal of **Ho-1** was observable but too weak for a reliable quantitative study.

The **Er-1** MC exhibits a typical long wavelength emission in the range of 1500−1600 nm, which originates from the $^4I_{13/2} \rightarrow {}^4I_{15/2}$ transition. The quantum yield in the solid state is equal to or slightly higher than the value observed for the previously reported $ErZn_{16}$ MC complex, $4.4(1)\cdot10^{-2}$ % vs $4.2(1)\cdot10^{-2}$ %.[36] When recorded in CD_3OD, the quantum yield of $4.5(3)\cdot10^{-2}$ % of **Er-1** is definitively larger than the corresponding value obtained for $ErZn_{16}$ MC ($3.6(1)\cdot10^{-2}$ %).[36]

The emission spectrum of the **Tm-1** MC recorded on solid state sample (Figure 5, blue trace) shows two groups of characteristic sharp bands in the blue and in the red spectral ranges that are attributed to the $^1G_4 \rightarrow {}^3H_6$ and $^1G_4 \rightarrow {}^3F_4/{}^1D_2 \rightarrow {}^3H_4$ transitions, respectively. The signal of the first transition overlaps with a broad organic emission arising from the chromophoric ligands which is due to an incomplete ligand-to-Tm^{3+} and/or to a back energy transfer process. The NIR emission bands originating from Tm^{3+} could not be observed. It was also not possible to observe any characteristic Tm^{3+} visible or NIR emission originating from **Tm-1** samples in CH_3OH or CD_3OD solutions.

An Yb^{3+} emission signal was observed with an apparent maximum at 980 nm for **Yb-1** and is attributed to the $^2F_{5/2} \rightarrow {}^2F_{7/2}$ transition. The quantum yield measured for **Yb-1** in the solid state, 5.88(2) %, is the highest value reported today in respect to any other values for Yb^{3+} complexes formed with organic ligands containing C−H bonds. The quantum yield drops slightly to a value of 4.29(1) % in CD_3OD. In CH_3OH, a significant decrease of the signal was observed, with a quantum yield determined to be 0.26(1) %.

The change of the luminescence lifetime values measured in a solvent and its deuterated derivative can be used to determine the hydration numbers (q) of the Ln^{3+} ions by applying phenomenological equations.[47−49] This study was performed for the Sm^{3+}, Tb^{3+}, Dy^{3+} and Yb^{3+} MCs. Results obtained with this series of lanthanide(III) cations of different types are in a good agreement (q = 0.7−1.2, Table 1), which indicates that one solvent molecule coordinates to the Ln^{3+} ion in solution.

Radiative Lifetimes of Yb^{3+} MC. With respect to Yb^{3+}, transitions generating the luminescence terminate onto the ground level. So the absorption spectrum corresponding to the emission spectrum in the range of the $^2F_{5/2} \leftarrow {}^2F_{7/2}$ transition can be measured (Figure 6) and used for the calculation of radiative lifetimes with the help of the modified Einstein's equations:[50]

$$\frac{1}{\tau_{rad}} = 2303 \times \frac{8\pi c n^2 \tilde{\nu}_m^{\,2}(2J+1)}{N_A(2J'+1)} \int \varepsilon(\tilde{\nu})\, d\tilde{\nu} \tag{1a}$$

$$\tilde{\nu}_m = \frac{\int \tilde{\nu}\varepsilon(\tilde{\nu})\, d\tilde{\nu}}{\int \varepsilon(\tilde{\nu})\, d\tilde{\nu}} \tag{1b}$$

where c is the speed of light in $cm\cdot s^{-1}$, n is the refractive index ($n(CH_3OH)$ = 1.329), N_A is Avogadro's number, J and J' are the quantum numbers for the ground and the excited states, respectively, $\int \varepsilon(\tilde{\nu})\, d\tilde{\nu}$ is the integrated spectrum of the $^2F_{5/2} \leftarrow {}^2F_{7/2}$ transition, $\tilde{\nu}_m$ is the barycenter of the transition. The results are summarized in Table 2.

DOI: 10.1021/jacs.6b00984
J. Am. Chem. Soc. 2016, 138, 5100−5109

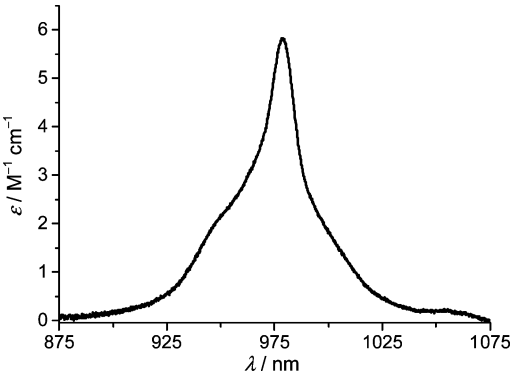

Figure 6. Absorption spectrum of the **Yb-1** MC in the energy range of $^2F_{5/2} \leftarrow {}^2F_{7/2}$ transition in CH_3OH at room temperature (1.8 mM).

Table 2. A Comparison of the Photophysical Properties of Yb^{3+} MCs[a]

compound	state/ solvent	τ_{obs} (μs)	τ_{rad} (ms)[b]	Q_{Yb}^{Yb} (%)	Q_{Yb}^{L} (%)	η_{sens} (%)
Yb-1	Solid	55.7(3)	0.37	15.1	5.88(2)	39
	CD_3OD	36.6(1)	0.53	6.9	4.29(1)	62
	CH_3OH	2.06(4)	0.53	0.39	0.26(1)	67
$YbZn_{16}$[c]	Solid	47.8(4)	0.47	10.2	2.44(4)	24
	CD_3OD	150.7(2)	0.68	22.2	2.88(2)	13
	CH_3OH	14.88(1)	0.68	2.2	0.25(1)	11

[a] 2σ values are given between parentheses, they refer to the reproducibility of the measurements. Experimental relative errors: τ_{obs}, ±2%; Q_{Yb}^{L}, ±10%; τ_{rad}, ±10%; Q_{Yb}^{Yb}, ±12%; η_{sens}, ±22%. [b] Determined using Yb^{3+}-centered absorption bands in CH_3OH (Figure 6) according to ref 50. For CD_3OD solutions and solid state, τ_{rad} was recalculated assuming that the structures are similar in the different media and taking into account the $1/n^3$ dependence of the refractive index, $n(CD_3OD)$ = 1.326, n(solid state) = 1.5. [c] For $Ln^{3+}[12\text{-}MC_{Zn(II),\ quinHA}\text{-}4]_2[24\text{-}MC_{Zn(II),\ quinHA}\text{-}8](OTf)_3$ from ref 36.

DISCUSSION

The MC topology has several advantages over other lanthanide(III) complexes formed by the direct coordination of chromophoric ligands to the metal ion: (i) the diamagnetic metal ions embedded in the MC ring form a rigid shell around the Ln^{3+} ion, which allows the control of a fixed distance between the Ln^{3+} ion and the C−H and O−H oscillators located on ligands and solvent molecules, thus promoting high intrinsic quantum yields, (ii) the Ln^{3+} ions are firmly encapsulated within the MC, which is important for in vivo applications where the toxicity of heavy metal-ions has an impact, (iii) the ligands can be easily modified for different study purposes. However, the a priori design of coordination complexes is not straightforward. In the case of Ga^{3+}, coordination from a ligand to oxygen or nitrogen is not enhanced by crystal-field stabilization energy and a variety of structures can be obtained. Thus, we approached the syntheses of **Ln-1** complexes in a targeted design.

The Ga^{3+} and Mn^{3+} metal ions are comparable in size (r = ~0.062 nm).[51] A 12-MC-4 metallacrown complex of Mn^{3+} and Ln^{3+} formed by employing shi^{3-} and benzoate ligands was previously reported.[32,38,39] More importantly, the X-ray crystal structure of this $LnMn_4$ complex shows the complete encapsulation of the Ln^{3+} ions within the Mn_4 ring. No solvent coordinates to the Ln^{3+} ions in this structure, which is desired for luminescent lanthanide(III) complexes. It was hypothesized that the substitution of the diamagnetic Ga^{3+} ions for Mn^{3+} ions can yield MC complexes that are amenable for Ln^{3+} emission.

Thus, in our synthetic strategy, the reaction of H_3shi and nitrate salts of Ga^{3+} and Ln^{3+} in CH_3OH/pyridine followed by the addition of sodium benzoate yielded $LnGa_4$ complexes (e.g., **Ln-1**) that are structurally very similar to the $LnMn_4$ complexes. It should be noted that the stoichiometric ratio of the reagents in the reaction mixture should be controlled according to the nature of the Ln^{3+} ion in order to obtain MCs with the desired topology. Sm^{3+} is the largest Ln^{3+} ion that can be involved in the formation of MCs with the **Ln-1** structure.

Luminescence Properties. In the solid state, upon excitation at 350 nm, the **Ln-1** complexes (Ln^{3+} = Sm, Eu, Tb, Dy, Ho, Er, Tm, Yb) exhibited sharp emission bands that correspond to the f−f transitions of the different lanthanide(III) ions, which spanned the visible and the NIR spectral regions (Figure 5). In general, all of these complexes are remarkable by their unusually high quantum yields and long luminescence lifetimes (Table 1). The Q_{Yb}^{L} of 5.88% for **Yb-1** is the highest value reported in the literature for an Yb^{3+} complex containing C−H bonds. It is also worth noting that emission from the Ho^{3+} and Tm^{3+} ions are very rarely observed in coordination complexes;[16,18,56−60] yet, in the case of **Ln-1** MCs emission of Ho^{3+} and Tm^{3+}, could be clearly detected and quantified.[18,20−22,52−54] (Figure 5 and Table 1). Being able to sensitize these additional lanthanides is advantageous for applications as it allows for additional signals that could be used for the creation of a barcode marker[55] or for multiplex detection when several signals have to be monitored during the same experiment with a unique excitation wavelength.

Moreover, visible and NIR dual-emitting Sm^{3+} and Dy^{3+} ions were sensitized by the reported MC scaffold and quantitative characteristics in both spectral ranges were collected. Recently, these Ln^{3+} ions have received exponentially increased attention for novel applications in materials and in biosciences.[4,21,52,56−58] In CH_3OH and CD_3OD solutions, most of the Ln^{3+} ions were sensitized, with the exception of Eu^{3+} and Tm^{3+}. Emission could be detected for Ho^{3+} and Er^{3+} MCs in CD_3OD but not in CH_3OH. **Ln-1** MCs are stable in CD_3OD solution as suggested by ^1H NMR (Figure S5). In addition, the similarities in the position and crystal-field splitting of the emission bands reflect the similarities of the coordination environments around lanthanide(III) ions in the solid state and in CD_3OD/CH_3OH solutions (Figure 5).

In order to control the lanthanide(III) sensitization mechanism, several parameters have to be taken into account for the design of luminescent Ln^{3+} coordination complexes. A comprehensive overview of the processes that need to be optimized can be found in recent review articles.[59,60] Briefly, the global quantitative parameter, the total quantum yield under ligand excitation, Q_{Ln}^{L}, is defined by the following formula in eq 2:

$$Q_{Ln}^{L} = \eta_{sens} \cdot Q_{Ln}^{Ln} = \eta_{ISC} \cdot \eta_{et} \cdot \frac{\tau_{obs}}{\tau_{rad}} \quad (2)$$

where Q_{Ln}^{Ln} is the intrinsic quantum yield; η_{sens} reflects the sensitization efficiency and can be calculated as the product of the intersystem crossing (η_{ISC}) and the energy transfer (η_{et}) efficiencies. τ_{obs} and τ_{rad} are defined as being the observed and the radiative lifetimes, respectively. In order to optimize sensitization efficiency, energy loss has to be minimized during the transfer processes between the initially excited singlet state and the donor electronic state(s) of the ligands, as well as

DOI: 10.1021/jacs.6b00984
J. Am. Chem. Soc. 2016, 138, 5100−5109

between the latter and the accepting level of the Ln^{3+} ion. The energy position of the singlet state (S_1) in **Ln-1** MCs was determined from the edge of the absorption spectra, which corresponds to an energy of 29 850 cm^{-1} (335 nm). Therefore, the energy difference between the S_1 and the T_1 (22 170 cm^{-1}) levels is larger than 5000 cm^{-1}, which is often considered as favorable for an efficient intersystem crossing.

It is generally hypothesized that the long-lived triplet states are, in most cases, the feeding levels of the luminescent Ln^{3+} ions. With this hypothesis, the choice of the ligands may be limited for the design of a universal scaffold capable of sensitizing all visible- and NIR-emitting Ln^{3+} series, since the T_1 level has to be located higher in energy than the main Ln^{3+} resonance accepting levels, which range from 21,350 cm^{-1} ($^1G_4$) for Tm^{3+} to 6700 cm^{-1} ($^4I_{13/2}$) for Er^{3+}.[45,46] In the case of **Ln-1**, the energy of the triplet state (22 170 cm^{-1}) is potentially well-adapted in this respect; it is at sufficiently high energy to sensitize the entire range of usually luminescent Ln^{3+} ions. However, the energy difference between the donating triplet state and the accepting $^1G_4$ (21 350 cm^{-1}), $^4F_{9/2}$ (21 100 cm^{-1}), and $^5D_4$ (20 400 cm^{-1}) electronic levels of Tm^{3+}, Dy^{3+} and Tb^{3+}, respectively, is relatively small (<2300 cm^{-1}), which increases the probability of back energy transfer processes from the Ln^{3+} ions to the chromophoric ligands, resulting in the decrease of the overall quantum yield.

Indeed, for this system, experimental data indicate the presence of a back energy transfer with a residual ligand emission that could be observed for the **Tm-1** complex in the solid state and for the **Dy-1** complex in methanol solution. The existence of this back-energy transfer was also confirmed by the increase of luminescence lifetimes upon lowering the temperature from room temperature to 10 K, these values changed from 1.08(1) to 1.45(1) ms for **Tb-1** and a more pronounced increase from 21.2(1) to 95.9(2) μs for **Dy-1** (Table 1 and S3, Supporting Information). For **Tm-1**, τ_{obs} decreases from 1.47(1) μs at 293 K to 1.01(1) μs at 10 K suggesting that more complex temperature-dependent processes may participate for this ion. This matter was not investigated further at this point.

The possibility of the formation of charge transfer states at energy levels that allow them to quench Ln^{3+} luminescence cannot be excluded. In the case of the **Eu-1** MC, only very weak Eu^{3+} emission was observed in the solid state (Figure 5). The presence of ligand-to-metal charge transfer (LMCT) states caused the broadening and the red-shifting of the diffuse reflectance and excitation bands (Figure 4, S3 Supporting Information) and is responsible for the yellow color of the **Eu-1** powder.

One of the ways to quantify the sensitization efficiency is to establish the ratio between the total and the intrinsic quantum yields (eq 2). The latter can be measured by direct excitation of the lanthanide(III) ion. However, this process is inefficient due to the forbidden nature of most of the f−f transitions and their low molar absorption coefficients. In the case of **Sm-1** MC in the solid state, we could determine Q_{Sm}^{Sm} = 5.1(2) % in the visible range under direct excitation into $^4G_{5/2} \leftarrow {}^4I_{9/2,\ 11/2}$ transitions at 480 nm. Thus, η_{sens} = 2.46/5.1 = 0.48 or 48% for **Sm-1**. So far, no reliable values of Sm^{3+} sensitization efficiencies in complexes with organic ligands have been reported. In addition to measurements through the direct excitation of the f−f transitions, intrinsic quantum yields can also be calculated using the equation: $Q_{Ln}^{Ln} = \tau_{obs}/\tau_{rad}$. The τ_{obs} can be easily measured, but the determination of τ_{rad} is not as straightforward. It is worth noting here that the radiative lifetime is not a constant for each Ln^{3+}, and it depends on the Ln^{3+} coordination environment and on the transition involved.[61] Recently, this parameter is receiving an increased attention, as it has been shown to be a promising way to improve intensities of luminescence of visible- and NIR-emitting Ln^{3+} complexes.[62−64]

For the **Yb-1** MC, τ_{rad} (Table 2) was calculated based on eq 1, and requires the collection of an absorption spectrum in CH_3OH in the energy range of the $^2F_{5/2} \leftarrow {}^2F_{7/2}$ transition (Figure 6). The calculated τ_{rad} value of 0.53 ms leads to Q_{Yb}^{Yb} = 0.39% and a sensitization efficiency of 67%. In CD_3OD, the calculated intrinsic quantum yield of 6.9% is 18 times higher than the value obtained in CH_3OH, while the η_{sens} value remains the same within the experimental error, reflecting the similarities in the energy transfer processes in CH_3OH and CD_3OD solutions. In the solid state, both the intrinsic and total quantum yields of **Yb-1** increase, while the sensitization becomes 1.6-times less efficient, which is likely the result of the presence of additional nonradiative processes.

The comparison of these data with the ones obtained for the previously reported $YbZn_{16}$ MCs[36] (Table 2) revealed that the sensitization efficiency is significantly enhanced for **Yb-1**, by 4.8−6.1-fold in solution and 1.6-fold in the solid state. In addition, the radiative lifetime is 1.3 times shorter for **Yb-1** in comparison to the value obtained for the $YbZn_{16}$, i.e. 0.53 vs 0.68 ms measured in solution and 0.37 vs 0.47 ms for the solid state. With respect to the intrinsic quantum yield, its value is 1.5 times higher in the solid state for **Yb-1** than for $YbZn_{16}$ (15.1 vs 10.2%), but the situation is inverted in solution, where the Q_{Yb}^{Yb} value is inferior by 3.2−5.6-times for the former complex. This observation indicates that the Zn^{2+} based $YbZn_{16}$ MC scaffold provides a more efficient protection of the Yb^{3+} ion from sources of nonradiative deactivation in solution than for **Yb-1**.

Estimation of the hydration numbers using phenomenological equations (see footnote to Table 1) which utilizes the difference between experimental lifetimes in CH_3OH and CD_3OD, shows that one solvent molecule is coordinated to the Ln^{3+} in the **Ln-1** MC structure. This nonzero q value is detrimental for the luminescence intensity and characteristics (luminescence lifetimes and quantum yields), as overtones of high-energy O−H vibrations of the solvent molecule create an efficient route to the nonradiative deactivation. It should be noted that the size of the spatial centroid located between the four benzoate groups measured from the innermost aromatic hydrogen atoms is ∼2.3 Å. Although no electron density was observed in the crystallographic data in this region, this void space is sufficiently large to be occupied by a solvent molecule when the MC is placed in solution (Figure S6 Supporting Information). This situation contrasts with the case of the $LnZn_{16}$ MC scaffold, where no solvent molecules were coordinated to Ln^{3+} ion in solid state and in solution.[36] Such high-energy vibrations play an important role in the nonradiative quenching of Ln^{3+} luminescence, in particular for NIR-emitting Ln^{3+} because of the small energy gaps between emitting and ground levels requiring a lower number of overtones of vibrations to deactivate the excited states.[59,60] This phenomenon can be exemplified with the **Ln-1** MCs upon switching solvents from CD_3OD to CH_3OH: the total quantum yield values decrease by 1.2, 2.1/2.5, 9.2/11.2, and 16.5 fold respectively for Tb^{3+} (visible), Dy^{3+} (visible/NIR), Sm^{3+} (visible/NIR) and Yb^{3+} (NIR).

DOI: 10.1021/jacs.6b00984
J. Am. Chem. Soc. 2016, 138, 5100−5109

In addition to O−H and N−H vibrations, C−H oscillators can also significantly quench luminescence, especially for the NIR-emitting Ln^{3+} ions. On the basis of the X-ray crystal structure of **Dy-1**, the shortest Ln···C−H distance was found to be ∼4.4 Å. This value is slightly longer or comparable to the Ln···C−H distances (3.4−4.6 Å) normally observed in complexes of Ln^{3+} formed with aromatic carboxylates[65,66] or β-diketonates[67,68] and still shorter than found in the $LnZn_{16}$ MC structures previously reported (∼6 Å).[36,37] Nevertheless, the total quantum yields of **Yb-1** and $YbZn_{16}$ MCs in CH_3OH solution are comparable within the experimental error (Table 2). Thus, the reduced protection of the Yb^{3+} from sources of nonradiative deactivation pathways including C−H vibrations and a nonzero solvation number is compensated by a 6.1 fold improvement in the sensitization efficiency and 1.3 fold decrease of the radiative lifetime.

CONCLUSIONS

We have created a second family of outstandingly bright NIR emitting lanthanide complexes based on metallacrowns. More specifically, we have designed, synthesized and fully characterized a new family of visible and NIR-emitting $LnGa_4$ MCs with a nearly planar 12-MC-4 motif adopting a general formula, $[LnGa_4(shi)_4(C_6H_5CO_2)_4(C_5H_5N)(CH_3OH)]$ (Ln^{3+} = Sm, Eu, Gd, Tb, Dy, Ho, Er, Tm, Yb; H_3shi = salicylhydroxamic acid; **Ln-1**).

With respect to the previously described Zn^{2+} based MC that was a breakthrough in term of luminescence intensity ($LnZn_{16}$ complexes),[36] the use of Ga^{3+} associated with different ligands has a significant impact on the photophysical properties and overall maintains a globally high level of brightness. A major enhancement has been obtained by the sensitization of a larger number of luminescent lanthanide(III) cations. Indeed, we have shown here that the electronic structure of the H_3shi-based MCs is remarkable in its ability to sensitize several Ln^{3+} ions emitting in the visible (Eu^{3+}, Tb^{3+}), in the NIR (Ho^{3+}, Er^{3+}, Tm^{3+}, Yb^{3+}) and those able to emit in both visible and NIR (Sm^{3+} and Dy^{3+}) regions. Detailed analysis of the photophysical properties of **Yb-1** allows us to conclude that there is a significantly improved sensitization efficiency and a shortening of the radiative lifetime of this new MC scaffold in comparison to the family of the $LnZn_{16}$ complexes that we have previously reported.[36] Therefore, as of today, the **Yb-1** MC possesses the highest total quantum yield value in the solid state reported for Yb^{3+} complexes formed with organic ligands containing C−H bonds.

Luminescence lifetime analysis has shown a drawback in this Ga^{3+} based system in comparison to the Zn^{2+} MCs: the change of structure has induced a loss of the protection of the lanthanide(III) against the quenching induced by solvent molecule when the MCs are placed in solution. This quenching is responsible for a decrease in luminescence intensity which could potentially limit the applications of these lanthanide(III) complexes in protic solvents.

Nevertheless, the new luminescent MCs described in this work, with a special attention focused on the NIR-emitting Yb^{3+} or combined visible/NIR-emitting Sm^{3+} and Dy^{3+} analogues, have already highly attractive properties for bioanalytical and biological imaging applications.

In conclusion, this novel MC design strategy has been demonstrated to be a very promising approach for the creation of luminescent complexes. As the next steps, we will focus on strategies to improve the protection of the Ln^{3+} ions against nonradiative deactivation from solvent and ligand molecules, to control sensitization efficiencies, to shorten radiative lifetimes and to optimize the excitation wavelength for the desired applications. Ultimately, our goal is to establish a global rationale based on a set of rules for constructing exceptionally bright luminescent materials for biological imaging and other applications including material sciences.

ASSOCIATED CONTENT

Supporting Information

The Supporting Information is available free of charge on the ACS Publications website at DOI: 10.1021/jacs.6b00984.

Crystal data. (CIF)

Supplementary tables, figures, and X-ray crystallographic parameters. (PDF)

AUTHOR INFORMATION

Corresponding Authors

*svetlana.eliseeva@cnrs.fr

*stephane.petoud@inserm.fr

*vlpec@umich.edu

Present Addresses

[⊥]Department of Chemistry, Oakland University, Rochester, Michigan 48309, United States.

[∥]Department of Inorganic, Applied and Analytical Chemistry, University of Geneva, 1211 Geneva 4, Switzerland.

Author Contributions

[#]C.Y.C. and S.V.E. contributed equally to this work.

Notes

The authors declare no competing financial interest.

ACKNOWLEDGMENTS

The research leading to these results have received funding from the European Community's Seventh Framework Programme (IRSES Metallacrown: FP7/2007-2013) under grant agreement no. 611488. This research was also supported in US in part by the National Science Foundation under grant CHE-1361779, La Ligue contre le Cancer and La Région Centre. E.R.T. thanks the Burroughs Wellcome Fund CRTG. S.P. acknowledges support from the "Institut National de la Santé et de la Recherche Médicale" (INSERM). The work in France was carried out in the frame of COST actions (TD1004 and CM1006).

REFERENCES

(1) Verwilst, P.; Eliseeva, S. V.; Vander Elst, L.; Burtea, C.; Laurent, S.; Petoud, S.; Muller, R. N.; Parac-Vogt, T. N.; De Borggraeve, W. M. *Inorg. Chem.* **2012**, *51*, 6405.

(2) Bonnet, C. S.; Buron, F.; Caillé, F.; Shade, C. M.; Drahoš, B.; Pellegatti, L.; Zhang, J.; Villette, S.; Helm, L.; Pichon, C.; Suzenet, F.; Petoud, S.; Tóth, É. *Chem. - Eur. J.* **2012**, *18*, 1419.

(3) Foucault-Collet, A.; Gogick, K. A.; White, K. A.; Villette, S.; Pallier, A.; Collet, G.; Kieda, C.; Li, T.; Geib, S. J.; Rosi, N. L.; Petoud, S. *Proc. Natl. Acad. Sci. U. S. A.* **2013**, *110*, 17199.

(4) Foucault-Collet, A.; Shade, C. M.; Nazarenko, I.; Petoud, S.; Eliseeva, S. V. *Angew. Chem., Int. Ed.* **2014**, *53*, 2927.

(5) D'Aléo, A.; Bourdolle, A.; Brustlein, S.; Fauquier, T.; Grichine, A.; Duperray, A.; Baldeck, P. L.; Andraud, C.; Brasselet, S.; Maury, O. *Angew. Chem., Int. Ed.* **2012**, *51*, 6622.

(6) Suffren, Y.; Zare, D.; Eliseeva, S. V.; Guénée, L.; Nozary, H.; Lathion, T.; Aboshyan-Sorgho, L.; Petoud, S.; Hauser, A.; Piguet, C. *J. Phys. Chem. C* **2013**, *117*, 26957.

(7) Zhang, Q. Y.; Huang, X. Y. *Prog. Mater. Sci.* **2010**, *55*, 353.

DOI: 10.1021/jacs.6b00984
J. Am. Chem. Soc. 2016, 138, 5100−5109

(8) van der Ende, B. M.; Aarts, L.; Meijerink, A. *Phys. Chem. Chem. Phys.* **2009**, *11*, 11081.
(9) Suzuki, H. *J. Photochem. Photobiol., A* **2004**, *166*, 155.
(10) Bünzli, J.-C. G.; Eliseeva, S. V. *J. Rare Earths* **2010**, *28*, 824.
(11) Bünzli, J.-C. G.; Comby, S.; Chauvin, A. S.; Vandevyver, C. D. B. *J. Rare Earths* **2007**, *25*, 257.
(12) Bünzli, J.-C.; Eliseeva, S. In *Lanthanide Luminescence*; Hänninen, P., Härmä, H., Eds.; Springer: Berlin, 2011; Vol. 7, p 1.
(13) Bünzli, J.-C. G. *Chem. Rev.* **2010**, *110*, 2729.
(14) Uh, H.; Petoud, S. *C. R. Chim.* **2010**, *13*, 668.
(15) Biju, S.; Gopakumar, N.; Bünzli, J.-C. G.; Scopelliti, R.; Kim, H. K.; Reddy, M. L. P. *Inorg. Chem.* **2013**, *52*, 8750.
(16) Petoud, S.; Muller, G.; Moore, E. G.; Xu, J. D.; Sokolnicki, J.; Riehl, J. P.; Le, U. N.; Cohen, S. M.; Raymond, K. N. *J. Am. Chem. Soc.* **2007**, *129*, 77.
(17) Caillé, F.; Bonnet, C. S.; Buron, F.; Villette, S.; Helm, L.; Petoud, S.; Suzenet, F.; Toth, E. *Inorg. Chem.* **2012**, *51*, 2522.
(18) Zhang, J.; Badger, P. D.; Geib, S. J.; Petoud, S. *Angew. Chem., Int. Ed.* **2005**, *44*, 2508.
(19) Biju, S.; Eom, Y. K.; Bünzli, J.-C. G.; Kim, H. K. *J. Mater. Chem. C* **2013**, *1*, 3454.
(20) Law, G. L.; Pham, T. A.; Xu, J. D.; Raymond, K. N. *Angew. Chem., Int. Ed.* **2012**, *51*, 2371.
(21) Wartenberg, N.; Raccurt, O.; Bourgeat-Lami, E.; Imbert, D.; Mazzanti, M. *Chem. - Eur. J.* **2013**, *19*, 3477.
(22) Quici, S.; Cavazzini, M.; Marzanni, G.; Accorsi, G.; Armaroli, N.; Ventura, B.; Barigelletti, F. *Inorg. Chem.* **2005**, *44*, 529.
(23) Mezei, G.; Zaleski, C. M.; Pecoraro, V. L. *Chem. Rev.* **2007**, *107*, 4933.
(24) Chow, C. Y.; Trivedi, E. R.; Pecoraro, V.; Zaleski, C. M. *Comments Inorg. Chem.* **2015**, *35*, 214.
(25) Cutland, A. D.; Malkani, R. G.; Kampf, J. W.; Pecoraro, V. L. *Angew. Chem., Int. Ed.* **2000**, *39*, 2689.
(26) Grant, J. T.; Jankolovits, J.; Pecoraro, V. L. *Inorg. Chem.* **2012**, *51*, 8034.
(27) Jankolovits, J.; Lim, C.-S.; Kampf, J. W.; Pecoraro, V. L. *Z. Naturforsch., B: J. Chem. Sci.* **2010**, *65*, 263.
(28) Lim, C.-S.; Jankolovits, J.; Zhao, P.; Kampf, J. W.; Pecoraro, V. L. *Inorg. Chem.* **2011**, *50*, 4832.
(29) Boron, T. T., III; Kampf, J. W.; Pecoraro, V. L. *Inorg. Chem.* **2010**, *49*, 9104.
(30) Stemmler, A. J.; Kampf, J. W.; Kirk, M. L.; Atasi, B. H.; Pecoraro, V. L. *Inorg. Chem.* **1999**, *38*, 2807.
(31) Deb, A.; Boron, T. T.; Itou, M.; Sakurai, Y.; Mallah, T.; Pecoraro, V. L.; Penner-Hahn, J. E. *J. Am. Chem. Soc.* **2014**, *136*, 4889.
(32) Zaleski, C. M.; Tricard, S.; Depperman, E. C.; Wernsdorfer, W.; Mallah, T.; Kirk, M. L.; Pecoraro, V. L. *Inorg. Chem.* **2011**, *50*, 11348.
(33) Zaleski, C. M.; Kampf, J. W.; Mallah, T.; Kirk, M. L.; Pecoraro, V. L. *Inorg. Chem.* **2007**, *46*, 1954.
(34) Zaleski, C. M.; Depperman, E. C.; Dendrinou-Samara, C.; Alexiou, M.; Kampf, J. W.; Kessissoglou, D. P.; Kirk, M. L.; Pecoraro, V. L. *J. Am. Chem. Soc.* **2005**, *127*, 12862.
(35) Chow, C. Y.; Bolvin, H.; Campbell, V. E.; Guillot, R.; Kampf, J. W.; Wernsdorfer, W.; Gendron, F.; Autschbach, J.; Pecoraro, V. L.; Mallah, T. *Chemical Science* **2015**, *6*, 4148.
(36) Trivedi, E. R.; Eliseeva, S. V.; Jankolovits, J.; Olmstead, M. M.; Petoud, S.; Pecoraro, V. L. *J. Am. Chem. Soc.* **2014**, *136*, 1526.
(37) Jankolovits, J.; Andolina, C. M.; Kampf, J. W.; Raymond, K. N.; Pecoraro, V. L. *Angew. Chem., Int. Ed.* **2011**, *50*, 9660.
(38) Lah, M. S.; Pecoraro, V. L. *J. Am. Chem. Soc.* **1989**, *111*, 7258.
(39) Azar, M. R.; Boron, T. T.; Lutter, J. C.; Daly, C. I.; Zegalia, K. A.; Nimthong, R.; Ferrence, G. M.; Zeller, M.; Kampf, J. W.; Pecoraro, V. L.; Zaleski, C. M. *Inorg. Chem.* **2014**, *53*, 1729.
(40) *CrystalClear 2.0*; R Corporation: Tokyo, Japan.
(41) Sheldrick, G. M. *Acta Crystallogr., Sect. A: Found. Crystallogr.* **2008**, *A64*, 112.
(42) Casanova, D.; Llunell, M.; Alemany, P.; Alvarez, S. *Chem. - Eur. J.* **2005**, *11*, 1479.
(43) Pasatoiu, T. D.; Madalan, A. M.; Kumke, M. U.; Tiseanu, C.; Andruh, M. *Inorg. Chem.* **2010**, *49*, 2310.
(44) Ganapathi, M.; Eliseeva, S. V.; Brooks, N. R.; Soccol, D.; Fransaer, J.; Binnemans, K. *J. Mater. Chem.* **2012**, *22*, 5514.
(45) Carnall, W. T.; Fields, P. R.; Rajnak, K. *J. Chem. Phys.* **1968**, *49*, 4447.
(46) Carnall, W. T.; Fields, P. R.; Rajnak, K. *J. Chem. Phys.* **1968**, *49*, 4424.
(47) Kimura, T.; Kato, Y. *J. Alloys Compd.* **1998**, *271*, 867.
(48) Horrocks, W. d., Jr.; Sudnick, D. R. *J. Am. Chem. Soc.* **1979**, *101*, 334.
(49) Beeby, A.; Clarkson, I. M.; Dickins, R. S.; Faulkner, S.; Parker, D.; Royle, L.; de Sousa, A. S.; Williams, J. A. G.; Woods, M. *J. Chem. Soc., Perkin Trans. 2* **1999**, 493.
(50) Werts, M. H. V.; Jukes, R. T. F.; Verhoeven, J. W. *Phys. Chem. Chem. Phys.* **2002**, *4*, 1542.
(51) Shannon, R. *Acta Crystallogr., Sect. A: Cryst. Phys., Diffr., Theor. Gen. Crystallogr.* **1976**, *32*, 751.
(52) Ahmed, Z.; Iftikhar, K. *J. Phys. Chem. A* **2013**, *117*, 11183.
(53) Martins, A. F.; Eliseeva, S. V.; Carvalho, H. F.; Teixeira, J. M.; Paula, C. T.; Hermann, P.; Platas-Iglesias, C.; Petoud, S.; Toth, E.; Geraldes, C. F. *Chem. - Eur. J.* **2014**, *20*, 14834.
(54) Moore, E. G.; Szigethy, G.; Xu, J.; Pålsson, L.-O.; Beeby, A.; Raymond, K. N. *Angew. Chem., Int. Ed.* **2008**, *47*, 9500.
(55) White, K. A.; Chengelis, D. A.; Gogick, K. A.; Stehman, J.; Rosi, N. L.; Petoud, S. *J. Am. Chem. Soc.* **2009**, *131*, 18069.
(56) Biju, S.; Eom, Y. K.; Bünzli, J.-C. G.; Kim, H. K. *J. Mater. Chem. C* **2013**, *1*, 6935.
(57) Biju, S.; Gopakumar, N.; Bünzli, J.-C. G.; Scopelliti, R.; Kim, H. K.; Reddy, M. L. P. *Inorg. Chem.* **2013**, *52*, 8750.
(58) Bui, A. T.; Grichine, A.; Brasselet, S.; Duperray, A.; Andraud, C.; Maury, O. *Chem. - Eur. J.* **2015**, *21*, 17757.
(59) Bünzli, J.-C. G.; Eliseeva, S. V. In *Comprehensive Inorganic Chemistry II*; Yam, V. W.-W., Ed.; Elsevier B.V.: Amsterdam, 2013; Vol. *8*, p 339.
(60) Bünzli, J.-C. G. *Coord. Chem. Rev.* **2015**, *293*−*294*, 19.
(61) Bünzli, J.-C. G.; Chauvin, A.-S.; Kim, H. K.; Deiters, E.; Eliseeva, S. V. *Coord. Chem. Rev.* **2010**, *254*, 2623.
(62) Doffek, C.; Seitz, M. *Angew. Chem., Int. Ed.* **2015**, *54*, 9719.
(63) Shavaleev, N. M.; Eliseeva, S. V.; Scopelliti, R.; Bünzli, J.-C. G. *Inorg. Chem.* **2015**, *54*, 9166.
(64) Shavaleev, N. M.; Scopelliti, R.; Gumy, F.; Bünzli, J.-C. G. *Inorg. Chem.* **2009**, *48*, 7937.
(65) Zhao, X.; Yu, X. Y.; Chen, T. L.; Luo, Y. H.; Yang, J. J.; Zhang, H. *Inorg. Chem. Commun.* **2012**, *20*, 247.
(66) Ramya, A. R.; Sharma, D.; Natarajan, S.; Reddy, M. L. P. *Inorg. Chem.* **2012**, *51*, 8818.
(67) Eliseeva, S. V.; Ryazanov, M.; Gumy, F.; Troyanov, S. I.; Lepnev, L. S.; Bünzli, J.-C. G.; Kuzmina, N. P. *Eur. J. Inorg. Chem.* **2006**, *2006*, 4809.
(68) Eliseeva, S. V.; Pleshkov, D. N.; Lyssenko, K. A.; Lepnev, L. S.; Bünzli, J.-C. G.; Kuzmina, N. P. *Inorg. Chem.* **2010**, *49*, 9300.

DOI: 10.1021/jacs.6b00984
J. Am. Chem. Soc. 2016, 138, 5100−5109